IFIT1 is rapidly evolving and exhibits disparate antiviral activities across 11 mammalian orders

Matthew B. McDougal[1], Anthony M. De Maria[1], Emi Nakahara[1], Ian N. Boys[1], and John W. Schoggins[1]*

[1]Department of Microbiology, University of Texas Southwestern Medical Center, Dallas, TX, USA

*To whom correspondence may be addressed. **Email:** john.schoggins@utsouthwestern.edu

Abstract

Mammalian mRNAs possess an N7-methylguanosine (m7G) cap and 2'O methylation of the initiating nucleotide at their 5' end, whereas certain viral RNAs lack these characteristic features. The human antiviral restriction factor IFIT1 recognizes and binds to specific viral RNAs that lack the 5' features of host mRNAs, resulting in targeted suppression of viral RNA translation. This interaction imposes significant host-driven evolutionary pressures on viruses, and many viruses have evolved mechanisms to evade the antiviral action of human IFIT1. However, little is known about the virus-driven pressures that may have shaped the antiviral activity of IFIT1 genes across mammals. Here, we take an evolution-guided approach to show that the IFIT1 gene is rapidly evolving in multiple mammalian clades, with positive selection acting upon several residues in distinct regions of the protein. In functional assays with 39 IFIT1s spanning diverse mammals, we demonstrate that IFIT1 exhibits a range of antiviral phenotypes, with many orthologs lacking antiviral activity against viruses that are strongly suppressed by other IFIT1s. We further show that IFIT1s from human and a bat, the black flying fox, inhibit Venezuelan equine encephalitis virus (VEEV) and strongly bind to Cap0 RNAs. Unexpectedly, chimpanzee IFIT1, which differs from human IFIT1 by only 8 amino acids, does not inhibit VEEV infection and exhibits minimal Cap0 RNA-binding. In mutagenesis studies, we determine that amino acids 364 and 366, with the latter undergoing positive selection, are sufficient to confer the differential anti-VEEV activity between human and chimpanzee IFIT1. These data suggest that virus-host genetic conflicts have influenced the antiviral specificity of IFIT1 across diverse mammalian orders.

Introduction

Interferon-induced protein with tetratricopeptide repeats 1 (IFIT1) is an interferon-stimulated gene (ISG) that is capable of distinguishing between self and non-self RNA. Mammalian mRNAs possess an N7-methylguanosine (m7G) cap and 2′O methylation of the initiating nucleotide at their 5’ end. Many viral RNAs, however, lack these characteristic features. IFIT1 is able to recognize and bind viral RNAs that lack a m7G cap, including 5’ triphosphate (5’-ppp-RNA) or viral RNAs that possess a m7G cap but lack 2′O methylation of the initiating nucleotide (Cap0 RNA) (1, 2). Crystal structures of human IFIT1 bound to both 5’-ppp-RNA and Cap0 RNA have helped uncover biochemical and structural determinants of IFIT1 antiviral activity, including residues that confer RNA-binding properties (3). IFIT1 binding to viral RNA subsequently inhibits infection by decreasing the amount of accessible RNA from the pool of replicating viral RNA (4) and by interacting with eIF proteins required for translation of viral proteins (5).

Viral restriction via IFIT1 binding to non-self RNAs imposes a host-driven evolutionary pressure for viruses to evade the antiviral function of IFIT1, as many viruses have evolved various mechanisms to elude IFIT1 binding and viral suppression (5). This includes viruses encoding their own capping and 2’O methyltransferase enzymes, using internal ribosome entry sites (IRES) to allow cap-independent translation of viral proteins, using host mRNA caps through cap-snatching, or hindering IFIT1 binding with RNA structures (5). For the alphavirus Venezuelan equine encephalitis virus (VEEV), which has a positive-sense, single-stranded RNA (+ssRNA) genome, a secondary RNA structure in the 5’ UTR of the pathogenic Trinidad strain occludes IFIT1 binding to viral RNA, whereas the IFIT1-sensitive TC-83 strain has a point mutation that destabilizes this RNA structure. This allows IFIT1 to bind viral RNA and inhibit viral infection (1). VEEV TC83 can be inhibited by both human IFIT1 and mouse Ifit1B, suggesting

100 similar mechanisms have been at least partially evolutionarily conserved to restrict viral infection
101 by IFIT proteins. However, as viruses have evolved mechanisms to evade IFIT1 antiviral activity,
102 IFIT1 may also experience evolutionary pressure to overcome viral evasion. We know little
103 about how such virus-imposed constraints may have influenced *IFIT1* evolution across
104 mammals, broadly.

105 Pathogenic viruses can cause severe disease or death in mammals, imposing a major
106 selective pressure on their mammalian hosts to evolve mechanisms that restrict viral infection.
107 In turn, there is pressure on viruses to evade host defenses. These “molecular arms races” of
108 host-pathogen co-evolution are evident as many genes involved in antiviral immunity exhibit
109 signatures of positive selection or rapid evolution. Computational evolutionary analyses of
110 antiviral ISGs have revealed specific domains and residues that are rapidly evolving (6-8).
111 Identifying these signatures of positive selection has uncovered functional determinants of
112 antiviral function in antiviral effectors such as MX1 and TRIM5α (9, 10). In addition to
113 evolutionary pressure from host-pathogen molecular arms races, IFIT1 may have also been
114 influenced by gene recombination occurring between *IFIT1* and the *IFIT1B* gene (11). *IFIT1*
115 genes have undergone duplication, gene loss, and recombination with *IFIT1B* in mammals,
116 resulting in genes that exhibit differential antiviral activity However, this was only assessed in a
117 few species, and the extent of differential antiviral activity of IFIT1 across Mammalia remains
118 unknown. Recently, in a screen for antiviral ISGs from bats, we found that IFIT1 from the black
119 flying fox displays particularly strong suppression of VEEV (12).

120 Together, these studies led us to hypothesize that evolution may have resulted in
121 “species-specific” antiviral ability of IFIT1 orthologs. While previous studies have provided
122 considerable insight into the antiviral mechanism and structure of some mammalian IFIT1
123 proteins, a comprehensive study into the antiviral specificity of IFIT1 orthologs remains lacking.

124 Accordingly, we sought to use evolutionary and functional methods to interrogate differences in
125 antiviral activity and biochemical properties of mammalian IFIT1.

126 **Results**

127 *IFIT1 is rapidly evolving in mammals*

128 Many antiviral effectors exhibit signatures of positive selection, as restriction factors and
129 the viruses they suppress are often engaged in "molecular arms races (6, 7)." Therefore, we
130 hypothesized IFIT1 may be rapidly evolving, as IFIT1 is a potent antiviral effector that many
131 viruses have evolved mechanisms to evade (5). To test this, we used established computational
132 methods to determine if the *IFIT1* gene is rapidly evolving across diverse clades of mammals.
133 Using Phylogenetic Analysis using Maximum Likelihood (PAML) (13), we determined that *IFIT1*
134 exhibits signatures of rapid evolution in all clades tested (primates, bats, carnivores, and
135 ungulates) (Fig 1A). Rodents were not included in this analysis, as a genetic ortholog of IFIT1
136 has been lost in many rodent species (11). While all lineages showed signs of rapid evolution,
137 carnivore IFIT1s exhibited the least significant likelihood of pervasive positive selection.
138 However, all mammalian lineages were also determined to have at least 2 sites of statistically
139 significant positive selection (Fig 1A). Detection of positive selection in certain domains or at
140 specific sites of restriction factors has been utilized to uncover genetic determinants of antiviral
141 function (6, 7). Therefore, we sought to potentially uncover other sites in IFIT1 that may be
142 engaged in host-pathogen conflicts using complementary methods to PAML. We next used Fast
143 Unconstrained Bayesian AppRoximation (FUBAR) (14), another approach that had been used
144 to identify rapidly evolving sites of restriction factors. Using FUBAR analysis, we further
145 identified at least one site predicted to be undergoing significant rapid evolution for all clades
146 except carnivores (Fig 1B). Another complementary analysis, Mixed Effects Model of Evolution
147 (MEME) (15), identified several sites of positive selection for all linages of tested mammals (Fig

148 1C). To our knowledge, these signatures of positive selection in *IFIT1* have not previously been
149 reported and suggest that evolutionary pressure has acted on multiple regions of IFIT1.

150 *Human IFIT1 residue 193 exhibits mutational resiliency*

151 We next focused on three codons in primate IFIT1 – encoding V170, L193, and L366 in
152 the human ortholog – that were determined by at least two models to be evolving under positive
153 selection (Fig 1D). We examined the location of each in solved IFIT1 structures for potential
154 importance in RNA-binding. None of these residues had previously been reported to be involved
155 in IFIT1 RNA-binding or antiviral function (2, 3). While crystal structures of human IFIT1 bound
156 to RNA indicate that residues V170 and L366 are not near the RNA-binding region, L193 is part
157 of the TPR4 loop which has been reported to act as a lid over the 3' exit of the RNA-binding
158 tunnel (3) (Fig 2A, 2B). The TPR4 loop, located between α-helices 9 and 10, also has been
159 suggested to play a role in mediating contacts between subdomain II and subdomain III (Fig 2B)
160 (3). Specifically, L193 in human IFIT1 protrudes into the exit of the RNA-binding tunnel and
161 comes into close contact with RNA (Fig 2C) (3). In addition, L193 is in close proximity to R187,
162 which is required for IFIT1 RNA binding and antiviral function (2). Therefore, we sought to test
163 the importance of L193 in the antiviral function of IFIT1. Our general strategy was to use
164 CRISPR-Cas9 gene editing to silence endogenous IFIT1 in human cells, and then reconstitute
165 expression by ectopic expression of IFIT1 193 mutants. We performed site-directed
166 mutagenesis to generate point mutations in a CRISPR-resistant human IFIT1 clone that
167 correspond to every possible amino acid at residue 193. Huh7.5 cells that were CRISPR-
168 targeted for endogenous IFIT1 were transduced with lentiviral pseudoparticles to express each
169 of the 193 mutant IFIT1s or appropriate controls. Cells expressing the IFIT1 point mutants were
170 then challenged with VEEV encoding a GFP reporter, and infection was quantified by flow
171 cytometry (Fig 2D). We observed that most amino acid substitutions at residue 193 were

172 tolerated by human IFIT1 with respect to antiviral function. In addition, western blotting
173 determined that all IFIT1 point mutants were expressed to appreciable levels (Fig 2D, Bottom).
174 Indeed, all mutants at position 193, whether hydrophobic or positively charged, inhibited VEEV
175 similarly to the wild-type (193L) IFIT1 (Fig 2D). Polar amino acids introduced at position 193
176 also retained antiviral function (Fig 2D). Severe loss of function in anti-VEEV activity of IFIT1
177 was only notable with glycine or proline (~50% loss of antiviral function) or with negatively
178 charged residues (~75-100% loss of antiviral function) (Fig 2D). This experiment demonstrated
179 the resiliency of IFIT1 antiviral function despite introduction of mutations in rapidly evolving site
180 193 within the TPR4 loop.

181 *IFIT1 orthologs from diverse mammals demonstrate species-specific antiviral activity*

182 To better understand the consequences of the evolutionary pressures on IFIT1, we
183 sought to test the antiviral activity of diverse mammalian IFIT1 orthologs against RNA viruses.
184 To accomplish this, we cloned IFIT1 protein-coding sequences from 38 species (including 2
185 predicted IFIT1 sequences from horse) of mammals into lentiviral expression vectors. The
186 chosen orthologs ranged from 60% to over 98% identical to human IFIT1 in protein coding
187 sequence and encompassed 11 taxonomic orders (Fig 3A, Fig 3B, Supp Table 1) within the
188 superorders Euarchontoglires, Laurasiatheria, Afrotheria, and Xenartha, thus representing
189 extensive diversity in both sequence and evolutionary distance relative to human IFIT1. All IFIT1
190 orthologs were also N-terminally HA-tagged to allow for detection by western blot. After
191 generating lentivirus pseudoparticles, we transduced human Huh7.5 cells with these 39 IFIT1
192 orthologs or appropriate controls and challenged IFIT1-expressing cells with two different RNA
193 viruses encoding a GFP reporter, VEEV and vesicular stomatitis virus (VSV) . These viruses
194 were chosen because of reported suppression by human IFIT1 through distinct mechanisms.
195 VSV is a rhabdovirus with a negative sense single-stranded RNA genome. IFIT1 inhibits VSV by

196 binding to viral RNA ending in a triphosphate (5'-ppp-N), sequestering viral RNA from the
197 replicating RNA pool (2). VEEV (TC-83 strain) is an alphavirus with a positive-sense single-
198 stranded RNA genome and is restricted by IFIT1 due to the binding and translation inhibition of
199 viral Cap0 RNA (m7G-ppp-N). This viral RNA possesses the canonical m7G cap but lacks 2'O
200 methylation of the initialing nucleotide of the viral 5' UTR, allowing recognition and binding by
201 human IFIT1 (1, 16). IFIT1-expressing cells were challenged with an MOI of 1 for both VSV-
202 GFP and VEEV-GFP, and infection was quantified by flow cytometry (Fig 3C). IFIT1 orthologs
203 capable of potently restricting VSV or VEEV infection, defined by inhibition of 70% or greater
204 relative to control cells, were considered hits in this screen. VEEV infection was potently
205 suppressed by eleven IFIT1 orthologs (African savannah elephant, Chinese pangolin, sheep,
206 white-tailed deer, black flying fox, dromedary camel, orca, Angola colobus, big brown bat,
207 human, and large flying fox) (Fig 3C). Five IFIT1 orthologs (orca, cape elephant shrew, dolphin,
208 European rabbit, and nine-banded armadillo) inhibited VSV infection by at least 70% compared
209 to control cells (Fig 3D). We were surprised that hits for each virus spanned such diverse
210 mammalian clades, and that there was little overlap in orthologs that inhibit VEEV and VSV. Also
211 unexpected, many IFIT1 orthologs exhibited no antiviral activity against these two viruses, as
212 only 10 of the 39 tested orthologs met our threshold to be considered hits. Western blotting
213 determined that IFIT1 expression was not uniform during the ortholog screen (Supp Fig 1),
214 suggesting that low expression of certain orthologs may have contributed to lack of antiviral
215 function. Expression of certain IFIT1 orthologs (e.g. orca and European rabbit) was much higher
216 than others, and some IFIT1 orthologs were expressed at very low levels (e.g. African green
217 monkey and greater horseshoe bat) (Supp Fig 1). In addition, black-capped squirrel monkey
218 IFIT1 was observed to run at a lower-than-expected molecular weight, suggesting a truncation
219 or cleavage of the protein product (Supp Fig 1). However, it was noted that many IFIT1
220 orthologs were hits in the screens despite low expression, and only orca IFIT1 was a hit in both

221 VSV and VEEV screens despite very high expression by multiple orthologs. These data suggest
222 that IFIT1 orthologs may exhibit species-specific antiviral functions independent of differences in
223 protein expression.

224 Since expression of IFIT1 from distinct species was not equal during the ortholog
225 screen, we sought to validate the antiviral phenotypes of a subset of orthologs with more
226 comparable expression. We selected 9 orthologs for follow-up based on protein expression,
227 evolutionary diversity, and variable phenotypes exhibited in the ortholog screen. Those chosen
228 for validation and follow-up included IFIT1 from Chinese pangolin (hereafter referred to as
229 pangolin), orca, sheep, black flying fox, big brown bat, chinchilla, human, chimpanzee, and cape
230 elephant shrew (hereafter referred to as shrew) (Fig 4A). Human Huh7.5 cells were transduced
231 with differing doses of lentivirus pseudoparticles to normalize IFIT1 expression between this
232 subset of orthologs. After puromycin selection, western blot analysis revealed that the
233 expression of IFIT1 orthologs was relatively uniform, except for the higher expression of orca
234 IFIT1 and notably lower expression of pangolin IFIT1 (Fig 4B). IFIT1-expressing cells were then
235 challenged with VEEV (Fig 4C) and VSV (Fig 4D) at an MOI of 2 to validate results from the
236 original IFIT1 ortholog overexpression screen. VSV was potently inhibited by orca and shrew
237 IFIT1, while no other tested orthologs significantly suppressed infection. Thus, VSV may evade
238 suppression by many mammalian IFIT1s. VEEV was potently inhibited by pangolin, sheep,
239 black flying fox, big brown bat, and human IFIT1, while orca IFIT1 modestly inhibited VEEV.
240 Strikingly, VEEV was not significantly inhibited by chimpanzee IFIT1 but was largely suppressed
241 by human IFIT1. This was of keen interest as human and chimpanzee IFIT1 differ in protein
242 sequence by only 8 amino acids, and one of these (residue 366) was identified as rapidly
243 evolving by both FUBAR and MEME (Fig 1D). Together, these validation experiments
244 demonstrate that mammalian IFIT1 species-specific differences in viral suppression are largely
245 independent of expression differences. This is exemplified by potent restriction of VEEV by

246 pangolin and big brown bat IFIT1 despite low expression (Fig 4B and 4C). Furthermore, high-
247 expressing sheep IFIT1 only restricted VEEV infection, but not VSV, and orca IFIT1 only
248 modestly reduced VEEV infection despite much higher expression than all other IFIT1s (Fig 4B-
249 D).

250 We further tested the ability of this subset of 9 IFIT1 orthologs to inhibit human
251 parainfluenza virus type 3 (PIV3) (Fig 4E). PIV3 is a paramyxovirus with a negative sense,
252 single-stranded RNA (-ssRNA) genome that is not previously reported to be inhibited by IFIT1.
253 However, PIV3 was chosen for follow-up because human IFIT1 is a dominant antiviral effector
254 towards the related human parainfluenza virus type 5 (PIV5) acting through an unknown
255 mechanism (17). PIV3 was significantly restricted by shrew, pangolin, chinchilla, black flying fox,
256 and big brown bat IFIT1 (Fig 4E). This was notable as human IFIT1 exhibited no antiviral activity
257 towards PIV3, whereas it is a key component of IFN-mediated restriction of the related PIV5
258 (17). Chinchilla IFIT1 also exhibited disparate activities, as it did not inhibit VEEV (Fig 4C) or
259 VSV (Fig 4D), yet significantly protected cells from PIV3 infection (Fig 4E). We then tested cells
260 expressing the 9 selected IFIT1 orthologs for the ability to suppress another alphavirus related
261 to VEEV, Sindbis virus (SINV) (Fig 4E). SINV was largely resistant to most mammalian IFIT1s,
262 consistent with previous human IFIT1 studies (1, 16). However, SINV was potently suppressed
263 by orca IFIT1, and modestly suppressed by pangolin, sheep, and chinchilla IFIT1 (Fig 4E),
264 highlighting a pattern of suppression that was distinct across the 9 orthologs relative to the
265 alphavirus VEEV. Together, these data demonstrate that IFIT1 orthologs exhibit broad antiviral
266 phenotypes towards a panel of viruses with both +ssRNA and -ssRNA genomes (Fig 4G),
267 largely independent of differences in protein expression.

268 *Human, black flying fox, and chimpanzee IFIT1 protein exhibit species-specific RNA binding*

269 As previously highlighted, human and black flying fox IFIT1 significantly protected cells
270 from VEEV infection compared to a control, while chimpanzee IFIT1 did not (Fig 4C). The black
271 flying fox (*Pteropus alecto*), is a model megabat species that is a reservoir for zoonotic viruses
272 (18-20) and expresses restriction factors with unique antiviral activities (12, 21). While human
273 and black flying fox IFIT1 share only 69% identity, human and chimpanzee IFIT1 are over 98%
274 identical (Fig 3B, Supp Table 1). Therefore, IFIT1 from these three species were of particular
275 interest for functional studies. Accordingly, we sought to determine if this variability in restricting
276 VEEV was due to differences in Cap0 RNA-binding ability of IFIT1 orthologs.

277 To perform *in vitro* RNA-binding assays, recombinant IFIT1 proteins were generated
278 (Supp Fig 2). We then performed an electrophoretic mobility shift assay (EMSA) to investigate
279 the RNA-binding properties of three mammalian IFIT1 orthologs. RNA probes matching the first
280 41 nucleotides of the VEEV 5' UTR were generated for EMSA by *in vitro* transcription. Probes
281 were capped by the faustovirus capping enzyme (22) to generate 5' ends that resemble
282 physiological Cap0 VEEV RNAs. After incubation of IFIT1 protein with Cap0 RNA probes,
283 protein:RNA complexes were run on native gels, which were stained with a nucleic acid dye to
284 visualize band shifts (Fig 5A). Quantification of band shift intensity and area under the curve
285 analysis revealed that black flying fox IFIT1 exhibited the strongest RNA binding activity (Fig 5B,
286 5C). Human IFIT1 also bound VEEV RNA, but to a lesser extent than black flying fox IFIT1.
287 Little binding was observed by chimpanzee IFIT1, as band shift intensity was barely above that
288 of a human RNA-binding deficient control (human IFIT1-R187H) (2, 3) (Fig 5B, 5C). These
289 biochemical data are consistent with viral phenotypes (Fig 4C), suggesting that species-specific
290 antiviral activities of IFIT1s can be partly explained by RNA binding potential.

291 *Mutagenesis of primate IFIT1 reveals genetic determinants of IFIT1 antiviral function*

292 While human IFIT1 exhibited potent VEEV restriction and significant VEEV Cap0 RNA
293 binding, chimpanzee IFIT1 lacked these properties. Chimpanzee and human IFIT1 differ by only
294 8 amino acids (Fig 6A), prompting us to examine which residues underlie the phenotypic
295 differences. We performed site-directed mutagenesis to generate point mutations in both human
296 and chimpanzee IFIT1 that correspond to the divergent residues between the two proteins (Fig
297 6A). As 3 of the 8 residues, 362, 364, and 366, are in close proximity (Fig 6A), we also
298 generated a triple mutant IFIT1 that has these residues swapped between chimpanzee and
299 human IFIT1 (hereafter referred to as the 362/4/6 triple mut). Notably, one of these three sites,
300 L366 in humans and M366 in chimpanzee, was determined to be rapidly evolving in 2 of the
301 tested computational models (Fig 1D).

302 We transduced Huh7.5 cells with lentiviruses expressing wild type (WT), single point
303 mutant IFIT1s, or 362/4/6 triple mut IFIT1. After selection of transduced cells with puromycin,
304 stable cells were challenged with VEEV-GFP at an MOI of 2 and infectivity was quantified by
305 flow cytometry (Fig 6B). Western blotting demonstrated near uniform expression of all human
306 and chimpanzee IFIT1 mutants (Fig 6B). Cells expressing wild-type chimpanzee IFIT1 were
307 infected by VEEV at a rate of about 50%, similar to the approximately 60% infection rate
308 observed in control cells. WT human IFIT1-expressing cells were infected at a rate of less than
309 10%, demonstrating significant VEEV suppression. Interestingly, the only point mutation in
310 human IFIT1 that resulted in a significant loss of antiviral activity was L366M. Cells expressing
311 human IFIT1 with the L366M point mutant were infected at a rate roughly 4-fold higher than
312 cells expressing WT human IFIT1 (Fig 6B). Introduction of a Q364R mutation in human IFIT1
313 also resulted in a partial loss of antiviral function, although this was not statistically significant.
314 Furthermore, the 362/4/6 triple mut introduced into human IFIT1 resulted in a near complete
315 loss of anti-VEEV function of human IFIT1(Fig 6B). The reciprocal was true for chimpanzee
316 IFIT1, which significantly gained antiviral function when the M366L mutation was introduced.

317 Cells expressing chimpanzee IFIT1 M366L were roughly half as likely to be infected as cells
318 expressing the WT chimpanzee IFIT1 (Fig 6B). In addition, R364Q mutant chimpanzee IFIT1
319 resulted in a moderate increase in antiviral activity; however, this was not statistically significant
320 compared to wild-type chimpanzee IFIT1. Furthermore, the 362/4/6 triple mut chimpanzee IFIT1
321 potently suppressed VEEV infection at a nearly identical level to that of WT human IFIT1.
322 Together, we show that residues N362, Q364, and L366 in human IFIT1 are necessary for viral
323 suppression of VEEV. In addition, the mutations of S362N, R364Q, and M366L in combination
324 are sufficient for chimpanzee IFIT1 to gain potent antiviral function.

325 Amino acids 362, 364, and 366 are generally conserved across IFIT1 from 20 different
326 primate species (Fig 6C). Specifically, residue 366 is typically a hydrophobic amino acid, with 5
327 out of the 20 primate sequences analyzed having either a valine or methionine, as seen in
328 chimpanzee IFIT1, instead of a leucine, which is present in human IFIT1 (Fig 6C). This suggests
329 that leucine at position 366 might be important for robust antiviral function in primate IFIT1,
330 although further experiments are necessary to confirm this role. Additional support for the
331 importance of L366 comes from our findings that the only primate IFIT1, besides those of
332 chimpanzees and humans, which was expressed at appreciable levels during the screen was
333 that of the Angola colobus. This IFIT1 variant also potently inhibited VEEV infection and notably
334 contains a leucine at residue 366, similar to human IFIT1 (Fig 3C, Supp Fig 1). Glutamine is
335 conserved at site 364 in all primate species aligned except chimpanzee which encodes an
336 arginine (Q364R), introducing a positive charge. Point mutants of residue 364 in chimpanzee
337 and human IFIT1 exhibited moderate alterations in anti-VEEV function, though not statistically
338 significant, suggesting that this amino acid may have a minor role in antiviral restriction that
339 synergizes with L366.

340 To test if residues 364 and 366 synergize to confer antiviral specificity between human
341 and chimpanzee IFIT1, 364 and 366 double mutants (referred to as 364/6 double mut) were
342 generated for both chimpanzee and human IFIT1. Huh7.5 cells expressing to express wild-type
343 (WT), 364/6 double mut, or 362/4/6 triple mut IFIT1s of both chimpanzee and human IFIT1 were
344 then challenged with VEEV-GFP at an MOI of 2 and infection was quantified by flow cytometry
345 (Fig 6D). Western blotting demonstrated uniform expression of all human and chimpanzee IFIT1
346 mutants (Fig 6D). As in previous experiments, wild-type human IFIT1 strongly suppressed
347 VEEV infection while wild-type chimpanzee IFIT1 did not (Fig 6D). However, the 364/6 double
348 mut and 362/4/6 triple mut of human IFIT1 both had a near complete loss of antiviral capacity,
349 resulting in cells being infected at a similar rate as cells expressing the wild-type chimpanzee
350 IFIT1 (Fig 6D). These results suggest that residues 364 and 366, but not residue 362, in human
351 IFIT1 are necessary to confer anti-VEEV function. In contrast, cells expressing the 364/6 double
352 mutant or the 362/4/6 triple mutant of chimpanzee IFIT1 potently suppressed VEEV infection at
353 rates similar to those observed in cells expressing wild-type human IFIT1. No difference in
354 antiviral potency was observed between chimpanzee IFIT1 with the 364/6 double mut or 362/4/6
355 triple mut, suggesting again that residue 362 does not play a key role in the differential antiviral
356 properties of human and chimpanzee IFIT1. Together, these data indicate that out of 8 amino
357 acids that differ between human and chimpanzee IFIT1, sites 364 and 366, in combination,
358 comprise the underlying differences in anti-VEEV function.

359 We next examined the location of amino acids 364 and 366 in the solved crystal
360 structure of human IFIT1 bound to RNA and in the chimpanzee IFIT1 structure predicted by
361 AlphaFold. Residues 364 and 366 are located within the α-helix 18 within TPR7 of IFIT1 (Fig
362 6A, 6E). They are not predicted to contact RNA and are not located in direct proximity of the
363 RNA-binding pocket (Fig 6E, 6F), suggesting they may regulate IFIT1 function in an allosteric
364 manner.

365 **Discussion**

366 Here, combining evolutionary and functional data, we conclude that mammalian IFIT1s
367 are rapidly evolving viral restriction factors that exhibit species-specific antiviral activity.
368 Furthermore, differences between the ability of human and chimpanzee IFIT1 to restrict VEEV
369 led to the unexpected discovery that 2 residues in α-helices 18 within the TPR7 domain of IFIT1
370 may partially determine primate IFIT1 antiviral capacity. Swapping amino acids 364 and 366 of
371 the IFIT1 protein sequence between human and chimpanzee IFIT1, in combination, resulted in
372 reciprocal antiviral phenotypes (Fig 6B, 6D). The structures of human and chimp IFIT1 suggest
373 that these amino acids are not directly involved in RNA binding. Thus, they may be involved in
374 conformational changes of IFIT1 during RNA-binding or other allosteric effects, though
375 additional studies are needed to test this.

376 Our data also support a hypothesis in which the breadth of IFIT1 antiviral phenotypes
377 may be, at least partially, explained by differences in RNA-binding ability. VEEV infection was
378 most potently suppressed by black flying fox IFIT1, significantly inhibited by human IFIT1, and
379 unaffected by chimpanzee IFIT1 (Fig 4C). This trend was similarly observed in RNA binding
380 assays with a sequence identical to that of the Cap0 VEEV 5' UTR by EMSA (Fig 5). Black flying
381 fox IFIT1 exhibited the strongest binding of VEEV Cap0 RNA, pronounced binding was
382 observed by human IFIT1, with minimal VEEV Cap0 RNA binding by chimpanzee IFIT1 (Fig 5).
383 These data are consistent with previous studies showing that the ability of IFIT1 to bind viral
384 RNA is required for its antiviral function (4, 23).

385 The differential antiviral activity between IFIT1B and IFIT1 across several mammals was
386 previously demonstrated by Daugherty et al.(11). This study used phylogenetic approaches to
387 show that gene birth, gene loss and gene conversion occurred throughout
388 vertebrate *IFIT* genes, resulting in extensive genetic diversity (11). Furthermore, through viral

389 infection assays and a yeast growth assay, the authors suggest different RNA-binding properties
390 and disparate antiviral functions between primate IFIT1s and mouse Ifit1b (11). Our studies
391 significantly expand the diversity of mammalian IFIT1s interrogated for antiviral function.
392 Notably, based on our studies, IFIT1s across *Mammalia* are not universally antiviral against
393 VEEV and VSV. In fact, antiviral specificity of IFIT1 orthologs is possibly quite narrow and highly
394 dependent on which virus is being evaluated.

395 We additionally provide new data to support a model in which mammalian IFIT1s
396 spanning diverse orders are rapidly evolving, and that in primates, this is occurring at
397 functionally relevant sites that are not directly implicated in RNA binding. Our computational
398 studies also identified amino acid 193 as rapidly evolving and a mutational scanning determined
399 that this residue is mutationally resilient. This was similarly observed for TRIM5α, in which most
400 mutations within the v1 loop did not affect antiviral potency (24). In addition, alteration of charge
401 within the v1 loop of TRIM5α played a significant role in determining the antiviral outcome of
402 TRIM5α mutants (24). We similarly observed that introduction of negatively charged residues at
403 position 193 within the TPR4 loop of human IFIT1 ablated antiviral activity (Fig 2D). Therefore,
404 mutational resiliency within a rapidly evolving residue of primate IFIT1 suggests that alteration of
405 a single amino acid within restriction factor IFIT1 may not result in major gain or loss antiviral
406 function. This may maximize the potential for adaptation during evolutionary arms races with
407 viruses. However, we cannot rule out the potential major role of mutations at position 193 in
408 combination with other mutations in IFIT1. Together, our data suggest that positions 193 is
409 rapidly evolving in primates and may accommodate many different amino acids while retaining
410 antiviral function.

411 Our study does have several limitations, however. All IFIT1 ortholog screens were
412 performed by expressing IFIT1 from distinct species in human cells, which may potentially affect

413 natural antiviral function. For example, some IFIT1 orthologs may bind viral RNA, but not
414 interface with human proteins to effectively suppress translation, resulting in no antiviral activity
415 when expressed in human cells. Furthermore, our biochemical assays focus on IFIT1 binding to
416 Cap0 RNA only. This is due to comparative studies that have demonstrated IFIT1 has the
417 strongest affinity for Cap0 RNA when compared to other RNAs, such as ppp-RNA (3). This
418 allowed us to use human IFIT1 as a positive control for Cap0 RNA-binding with a strong signal-
419 to-noise for comparative RNA binding assays between IFIT1 orthologs that were successfully
420 purified. However, it is possible that differences in ppp-RNA binding may underlie differences in
421 the antiviral potency of IFIT1 towards viruses such as VSV and PIV3. This study also does not
422 address the possibility that differential viral evasion of IFIT1 proteins contributes to species-
423 specific antiviral activity. Furthermore, we have only provided genetic, but not biochemical or
424 structural evidence for underlying differences in chimpanzee and human IFIT1 RNA-binding and
425 antiviral activity. By mutagenesis assays we demonstrate that 2 amino acid changes confer
426 antiviral activity between chimpanzee and human IFIT1. Additional insight into the role of these
427 residues might be gained from molecular dynamics simulations using the crystal structure of
428 human IFIT1 bound to Cap0 RNA as a template. Comparisons with the 364/366 double mutant
429 might determine whether these substitutions alter conformational dynamics in a manner that
430 disfavors RNA binding.

431 Summarily, our findings underscore the notion that unbiased screening, investigations of
432 restriction factors from non-model mammalian species, and evolutionary-guided approaches
433 may uncover novel findings in host-pathogen interactions.

434

435 **Materials and Methods**

436 *Cells and cell culture*

437 Huh7.5 and 293T cells (from C. Rice, The Rockefeller University) were maintained in “complete”
438 DMEM (Gibco): DMEM supplemented with 10% FBS (Gibco) and 1× non-essential amino acids
439 (NEAA; Gibco). All derived stable cells expressing selectable markers were grown in complete
440 DMEM containing puromycin (Gibco; Huh7.5: 4μg/mL). All cells were incubated at 37°C in 5%
441 CO_2. All cell lines have been STR profiled and confirmed negative for mycoplasma
442 contamination by PCR testing (Venor GeM mycoplasma detection kit, Sigma).

443 *Viruses and viral infections*

444 Venezuelan equine encephalitis virus (TC-83 strain) infectious clone was obtained from I.Frolov.
445 VEEV-GFP stocks were generated as previously described (25). Briefly, infectious clone plasmid
446 was linearized, and RNA was in vitro transcribed with the mMESSAGE mMACHINE™ SP6
447 Transcription Kit (Invitrogen) followed by RNA clean-up with the MEGAclear™ Transcription
448 Clean-Up Kit (Invitrogen). BHK-21J cells (8 x 10^6 cells) were then electroporated with 5μg of in
449 vitro transcribed RNA and plated. Media was changed 18 h after plating, and the remaining
450 supernatant was collected 8 h post-media change. After centrifugation to remove cell debris,
451 virus-containing supernatants were aliquoted and stored at -80°C. Sindbis virus (SINV-GFP,
452 clone S300 from M. Heise) (26) was generated as previously described. Vesicular stomatitis
453 virus (VSV-GFP) (from J. Rose) and human parainfluenza virus type 3 (PIV3-GFP) (JS strain,
454 from Peter Collins) were propagated by passaging in BHK-21J cells and storing clarified
455 supernatants as virus stocks at -80°C. All viral infections were performed in DMEM
456 supplemented with 1% FBS and 1x non-essential amino acids at a total volume of 0.2mL in 24-
457 well tissue culture plates. After a 1 h incubation period, 0.3mL of complete DMEM was added to
458 all wells until harvest. For analysis of viral infection by flow cytometry, cells were dissociated
459 from the plate with 150μL Accumax (Innovative Cell Technologies) and then fixed in
460 paraformaldehyde at a final concentration of 1%. Cells were allowed to fix for at least 30 min at

461 4°C and subsequently centrifuged at 1500 x *g* for 5 min. Supernatant was removed from cell
462 pellets and fixed cells were then resuspended in FACS buffer (PBS [Gibco] supplemented with
463 3% FBS). Flow cytometry was performed on the Stratedigm S1000EON benchtop flow
464 cytometer, with analysis in FlowJo software.

465 *Cloning and plasmids*

466 IFIT1 coding sequences were obtained from the NCBI database. IFIT1 sequences were cloned
467 into the Gateway expression vector pSCRPSY (27). IFIT1 orthologs were synthesized as
468 gBlocks (IDT) with Gateway compatible DNA sequences and an N-terminal HA tag. Human and
469 chimpanzee IFIT1 point mutants were generated using site-directed mutagenesis PCR. Human
470 and chimpanzee IFIT1 362/4/6 triple mutants and 364/6 double mutants were generated by
471 Gibson cloning of gBlocks (IDT). For protein purification, IFIT1 protein coding sequences that
472 were codon-optimized for bacterial expression were cloned into a modified pET28a bacterial
473 expression vector, containing an N-terminal 6X-His tag followed by the yeast Sumo (smt3).

474 *Western Blotting*

475 Cells were lysed with M-PER (Mammalian Protein Extraction Reagent, Thermo Scientific)
476 containing 1x complete protease inhibitor cocktail (Roche) at 4°C for 5 min with intermittent
477 rocking. Lysate was then stored at -80°C. For running SDS-PAGE, lysate was thawed on ice,
478 and mixed to a final concentration of 1x SDS Loading Buffer (0.2 M Tris-Cl pH 6.8, 5% SDS,
479 25% Glycerol, 0.025% Bromophenol Blue, and 6.25% beta-mercaptoethanol). Samples were
480 run on 12% TGX FastCast acrylamide gels (Bio-Rad) or 4-20% Mini-PROTEAN® TGX™
481 precast protein gels (BioRad) and transferred to nitrocellulose membranes using a TransBlot
482 Turbo system (Bio-Rad). Membranes were blocked with 5% milk in 1x Tris Buffered Saline, with
483 Tween-20 (TBS-T [20mM Tris, 150mM NaCl, 0.1% Tween-20]) for at least 45min. Subsequent
484 incubation with primary antibody (at dilutions between 1:500 to 1:5000) diluted in 1% milk in

485 TBS-T was performed overnight, rocking at 4°C. Primary antibodies probing for GAPDH
486 (Proteintech Cat# 10494-1-AP, RRID:AB_2263076 or Proteintech Cat# 60004-1-Ig,
487 RRID:AB_2107436), IFIT1 (Proteintech Cat# 23247-1-AP, RRID:AB_2811269) and HA-tagged
488 IFIT1 (Biolegend Cat# 901502, RRID:AB_2565006) were used in this study. After incubation
489 with primary antibodies, membranes were washed 3 times with TBS-T by rocking for 5 min.
490 Secondary antibodies (Goat anti-Rabbit 800CW and Goat anti-Mouse 680RD [LI-COR] at
491 1:5000 dilutions) diluted in 1x TBS-T were incubated with membranes for at least 45 min.
492 Membranes were then washed 3 times with TBS-T by rocking for 5 min. Proteins were
493 visualized using the LI-COR Odyssey FC imaging system.

494 *Lentivirus production and transduction*

495 To generate lentivirus pseudoparticles, 350,000 293Ts were plated onto poly-lysine coated 6-
496 well plates. Lentiviral packaging plasmids expressing VSV-g and Gag-pol were then mixed with
497 SCRPSY plasmids at a ratio of 0.1µg:0.5 µg:2.5 µg, respectively. Plasmids were incubated for
498 20 min with a mix of XtremeGENE9 transfection reagent (Roche) and OptiMEM (Gibco).
499 Transfection complexes were then added to 293T cells in 1mL of DMEM supplemented with 3%
500 FBS dropwise. After 6 h of incubation, media was changed to 1.5 mL of DMEM supplemented
501 with 3% FBS. Supernatants containing lentiviral pseudoparticles were harvested at 48 and 72 h
502 post-transfection. Lentiviral pseudoparticles were then processed by adding 4µg/mL Polybrene
503 (Sigma), 20mM HEPES, centrifuging at 1500rpm for 5min to remove cell debris, and storing at -
504 80°C until transductions.

505 Lentivirus transductions were performed in 6-well plates after plating 350,000 cells (Huh7.5).
506 Final volume of transductions was either 1mL or 1.5mL of lentivirus mixed with “pseudoparticle”
507 DMEM (DMEM supplemented with 3% FBS, 4µg/mL Polybrene, and 20mM HEPES) After a 6 h
508 incubation at 37°C, 2mL of complete DMEM was added to all transductions. Transduced cells

509 were split into selection media 48h post-transduction and passaged for a minimum of three
510 passages in selection media.

511

512 *Protein Purification*

513 IFIT1 protein coding sequences that were codon-optimized for bacterial expression were cloned
514 into a modified pET28a bacterial expression vector, containing an N-terminal 6X-His tag
515 followed by the yeast Sumo (smt3). Plasmids were transformed into Rosetta DE3 cells.
516 Transformants were grown in Terrific Broth (TB) with 50 mg/L Kanamycin and 34 mg/L of
517 Chloramphenicol and Antifoam B at 37 °C. At the OD_{600} of 0.4, the temperature was lowered to
518 18 °C. Protein expression was induced at OD_{600}=3 by addition of IPTG to 0.4 mM final
519 concentration. Cells were harvested after an overnight incubation by centrifugation (OD_{600}=~8.5)
520 and lysed in the lysis buffer (50 mM Tris-HCl pH 8, 500 mM NaCl, 15 mM Imidazole, 1 mM
521 PMSF, 4 mM β-ME) by sonication. Cell lysates were cleared by centrifugation at 35,000 x g for
522 30 minutes. The cleared lysate was applied onto a gravity column with pre-washed Ni-NTA
523 resin. Resin was washed with 50 mM Tris-HCl pH 8, 1 M NaCl, 30 mM Imidazole, 4 mM β-ME.
524 Proteins were eluted with 50 mM Tris-HCl pH 8, 300 mM NaCl, 300 mM Imidazole, 2 mM DTT.
525 Proteins were treated with Ulp1 protease overnight to remove the Sumo tag and passed over a
526 size-exclusion column (HiLoad 16/600 Superdex 200 pg), equilibrated with 50 mM Tris 8.0, 150
527 mM NaCl, 1 mM DTT. Peak fractions were pooled, concentrated by ultrafiltration, and stored at -
528 80 °C until use. For SDS-PAGE gels of purified IFIT1 protein, 500nM of human, black flying fox,
529 chimpanzee, and human R187H mutant IFIT1 were boiled in 4X Laemmli Sample Buffer
530 (BioRad) with 1.25% BME and loaded into a 4-20% Mini-PROTEAN® TGX™ Precast Protein
531 Gel (BioRad). Gels were run and subsequently incubated in Coomassie stain (40% ethanol,
532 10% glacial acetic acid, 0.1% Coomassie R-250) for 1 hour and destained overnight (10%

533 ethanol, 7.5% glacial acetic acid). Gels were imaged with the ChemiDoc Imaging System
534 (BioRad).

535 *RNA Electrophoretic mobility shift assay*

536 Protein stock concentration of IFIT1 orthologs was determined by diluting protein 1:5 in 1x TBE
537 and measuring A280. Extinction coefficient was determined by ProtParam tool (Expasy), and
538 subsequently used to calculate and normalize protein concentrations between stocks.

539 Before loading, native gels (10% 19:1 Acrylamide: Bis-acrylamide, 25mM NaCl, 1x TBE,
540 0.0005% APS, 0.001% TEMED) were pre-run with 1x TBE in a cold room for at least 2.5 h.
541 While gels were pre-running, binding reactions were set up at room temperature after thawing
542 and keeping both RNA and protein stocks on ice. All dilutions of protein and RNA were in 1x
543 reaction buffer (50nM TRIS pH 8.0, 100mM NaCl, 1mM EDTA, 0.01mg/mL Heparin sodium
544 sulfate, 2.5% Glycerol). For binding reactions, 50nM of Cap0 RNA was mixed 1:1 with 0, 80,
545 160, 240, 320, and 400nM of purified IFIT1 protein in a final volume of 20μL and incubated at
546 room temperature for 20 min.

547 18 μL of RNA:Protein complexes were then run on pre-run native gels for 2.5 h at 100V in 1x
548 TBE in a cold room. Gels were then stained with 1x SYBR Gold stain (ThermoFisher Scientific)
549 diluted in 1x TBE for 20 min rocking at room temperature and imaged on a ChemiDoc Imaging
550 System (BioRad) with UV transillumination. Band intensity was subsequently analyzed using
551 ImageLab software (BioRad).

552 *In vitro transcription and 5' capping of RNA probes*

553 Uncapped RNA probes were generated using the T7 RiboMAX™ Express Large Scale RNA
554 Production System (Promega). Manufacturer instructions were modified for generating short
555 RNA probes. Briefly, 10μM of DNA oligos corresponding to the T7φ2.5 promoter sequence and

556 the complementary T7φ2.5 promoter sequence followed by the first 41nt of the VEEV TC-83
557 strain 5' UTR sequence. Oligos were boiled at 95°C for 2-3 min and then slow cooled to room
558 temperature to allow annealing. 1 μM of the annealed DNA oligos served as the template per
559 20μL T7 transcription reaction. RNA was purified according to manufacturer instructions using
560 phenol:chloroform nucleic acid extraction (Promega).

561 To generate Cap0 RNA, purified uncapped RNA probes were modified using the Faustovirus
562 Capping Enzyme (FCE) (NEB) using modified manufacturer instructions. Briefly, 100μL
563 reactions were composed of 20μL of uncapped RNA purified after T7 transcription (described
564 above), 0.2mM SAM, 1mM GTP, 7500U of FCE, 1x FCE reaction buffer, 80U RNasin® Plus
565 Ribonuclease Inhibitor (Promega), and nuclease-free water up to 100μL. Reactions were
566 incubated at 42°C for 4.5 h and then another 0.5 h at 50°C. Cap0 RNA was then purified using
567 the same phenol:chloroform nucleic acid extraction as performed after the T7 transcription
568 reaction (Promega). Cap0 RNA was determined to be at least 95% Cap0 RNA (m7GpppA) by
569 targeted LC/MS after Nuclease P1 (NEB) digestion at 37°C for 30 min followed by inactivation of
570 enzyme at 95°C for 2 min. LC/MS was performed by the UT Southwestern Preclinical
571 Pharmacology Core Facility.

572

573 *Computational Evolutionary Analysis*

574 IFIT1 coding sequences for all analyses were obtained from the NCBI database. Alignment of
575 multiple sequences was performed using MUSCLE and ClustalW implemented in MEGA X (28).
576 Maximum-likelihood trees were constructed in MEGA X, with standard settings. Trimmed
577 alignments were then generated (29), and when required, ALTER(30) was used to convert file
578 formats. MEME (31) and FUBAR (14) were performed with HyPhy (32) using the Datamonkey
579 web application (33). To perform PAML analysis, we used default settings with the F3x4 codon

frequency table within CodeML. Likelihood ratio tests were performed to compare model 7 versus model 8 and model 8 versus model 8a to determine the presence of positive selection. Bayes empirical Bayes testing was performed to determine specific residues that are adaptively evolving. Species trees were generated using the TimeTree database (34). FigTree software was then used to make trees shown in figures. Alignments and determination of amino acid identity to human IFIT1 was performed using ClustalOmega (35). Graphics comparing human and chimpanzee IFIT1 structures were generated using ChimeraX (36).

Statistical analysis

All statistical analyses were performed in GraphPad Prism 9. All graphs represent the mean of n=3 independent biological replicates with error bars representing standard deviation. ns, $p > 0.05$, *, $p < 0.05$, **, $p < 0.01$, ***, $p < 0.001$, and **** $p < 0.0001$.

Acknowledgements

We thank Adam Osinski and Gina Park in the lab of Vincent Tagliabracci for purifiying IFIT1 protein and for technical assistance with RNA EMSAs. This work was funded in part by the National Science Foundation Graduate Research Fellowship (2019274212 to M.B.M.) and grants to J.W.S: NIH Grant AI158124, The Welch Foundation (I-2013-20220331), the UT Southwestern High Impact / High Risk Grant, and an Investigator in the Pathogenesis of Infectious Disease Award from the Burroughs Wellcome Fund.

Author Contributions

M.B.M, A.M.D., and E.N. performed technical experiments. M.B.M. and I.N.B. performed computational evolutionary analysis. M.B.M and J.W.S conceptualized this study and designed experiments. M.B.M and J.W.S wrote and edited the manuscript. M.B.M and J.W.S obtained funding.

A

Clade	N	p-value (M7vsM8)	p-value (M8vsM8a)	omega (dN/dS)	Positively selected sites (BEB p>0.95)
Primate	20	0.0006088	0.0002588	0.53606	193, 200
Bat	9	0.000001492	0.000003884	0.58854	193, 196, 367
Carnivore	21	0.008238	0.02007	0.40348	3, 296
Ungulate	21	8.58E-15	3.73E-15	0.88076	28, 44, 194, 195, 196, 197, 198, 203, 245, 284, 302, 319, 321, 325, 329, 339, 370, 372, 407, 411, 417, 474

B

Clade	N	Positively Selected Sites (>0.95 Probability)
Primate	20	30, 170, 193, 240, 366
Bat	9	193
Carnivore	20	N/A
Ungulate	20	196, 325, 417

C

Clade	N	Positively Selected Sites (<0.05 threshold)
Primate	20	2, 136, 170, 251, 266, 366, 414
Bat	9	80, 84, 92, 115, 127, 131, 153, 193, 230, 232, 298, 351, 352, 466
Carnivore	20	3, 7, 11, 63, 322
Ungulate	20	109, 129, 190, 200, 264, 265, 266, 284, 295, 302, 325, 329, 339, 406, 417, 472

D

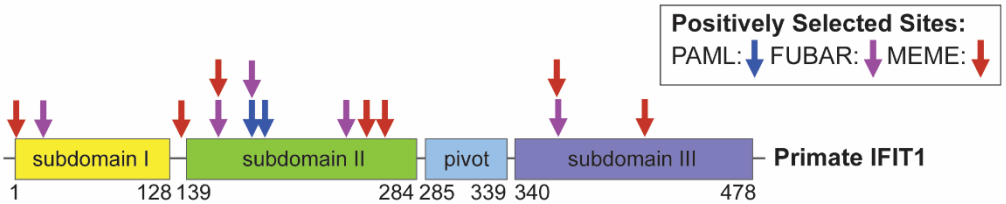

Figure 1. Evolutionary analysis of IFIT1 from clades of mammals reveals rapid evolution. A. PAML analysis on NCBI-derived coding sequences that were trimmed aligned using CodeML. Likelihood ratio tests were performed to compare model 7 vs model 8 and model 8 vs model 8a to determine the presence of positive selection. N=number of sequences input, and numbers under “positively selected sites” represent residue number of the reference sequence. B. FUBAR analysis on coding sequences that were trimmed and aligned using HyPhy software and DataMonkey. N=number of sequences input, and numbers under “positively selected sites” represent residue number of the reference sequence. C. MEME analysis on coding sequences that were trimmed and aligned using HyPhy software and the DataMonkey application. N=number of sequences input, and numbers under “sites of episodic positive selection” represent residue number of the reference sequence. D. Diagram of Primate IFIT1 domains and location of positively selected sites determined by PAML, FUBAR, and MEME.

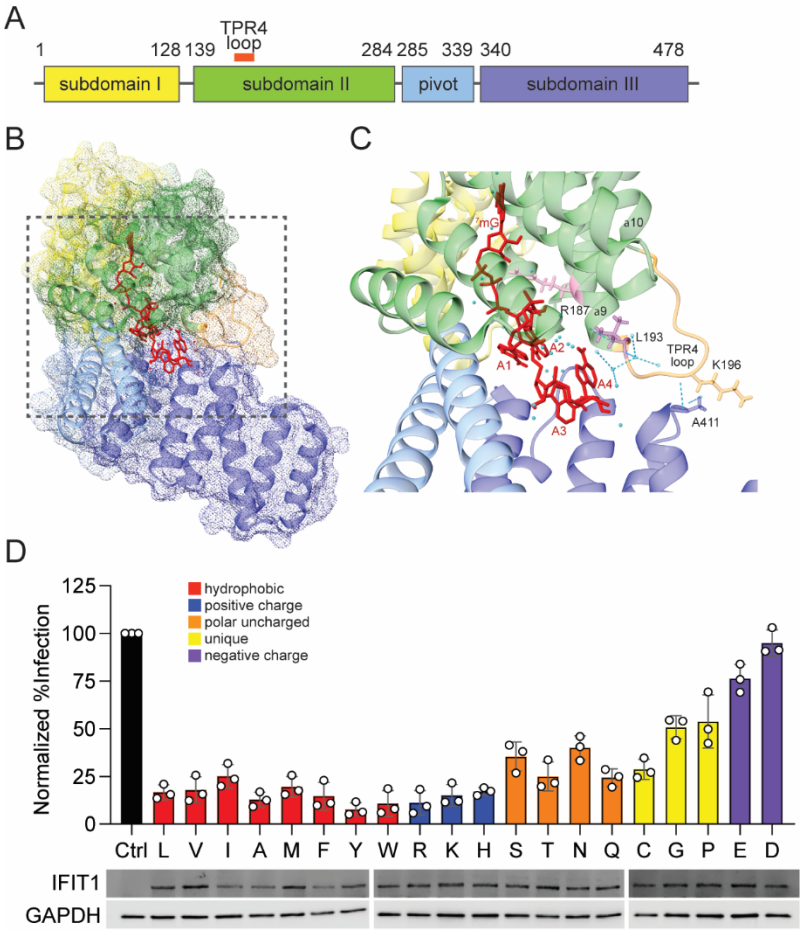

Figure 2. Mutagenesis of rapidly evolving residue 193 in human IFIT1 reveals mutational resiliency. A. Depiction of the human IFIT1 protein with the TPR4 loop location (orange) shown. B. Solved crystal structure of IFIT1 bound to RNA with TPR4 loop forming a "lid" over the exit of the RNA-binding tunnel (PDB:5udj). C. Zoom in on the TPR4 loop and RNA-binding tunnel exit illustrating the location of the TPR4 loop and residue 193 in relation to bound RNA in the human IFIT1 crystal structure. D. (Top) Saturating mutagenesis screen in cells expressing human IFIT1 with residue 193 mutated to every possible residue and challenged with VEEV infection. (Top) (Bottom) Western blot from lysates of Huh7.5 cells expressing IFIT1 point mutants.

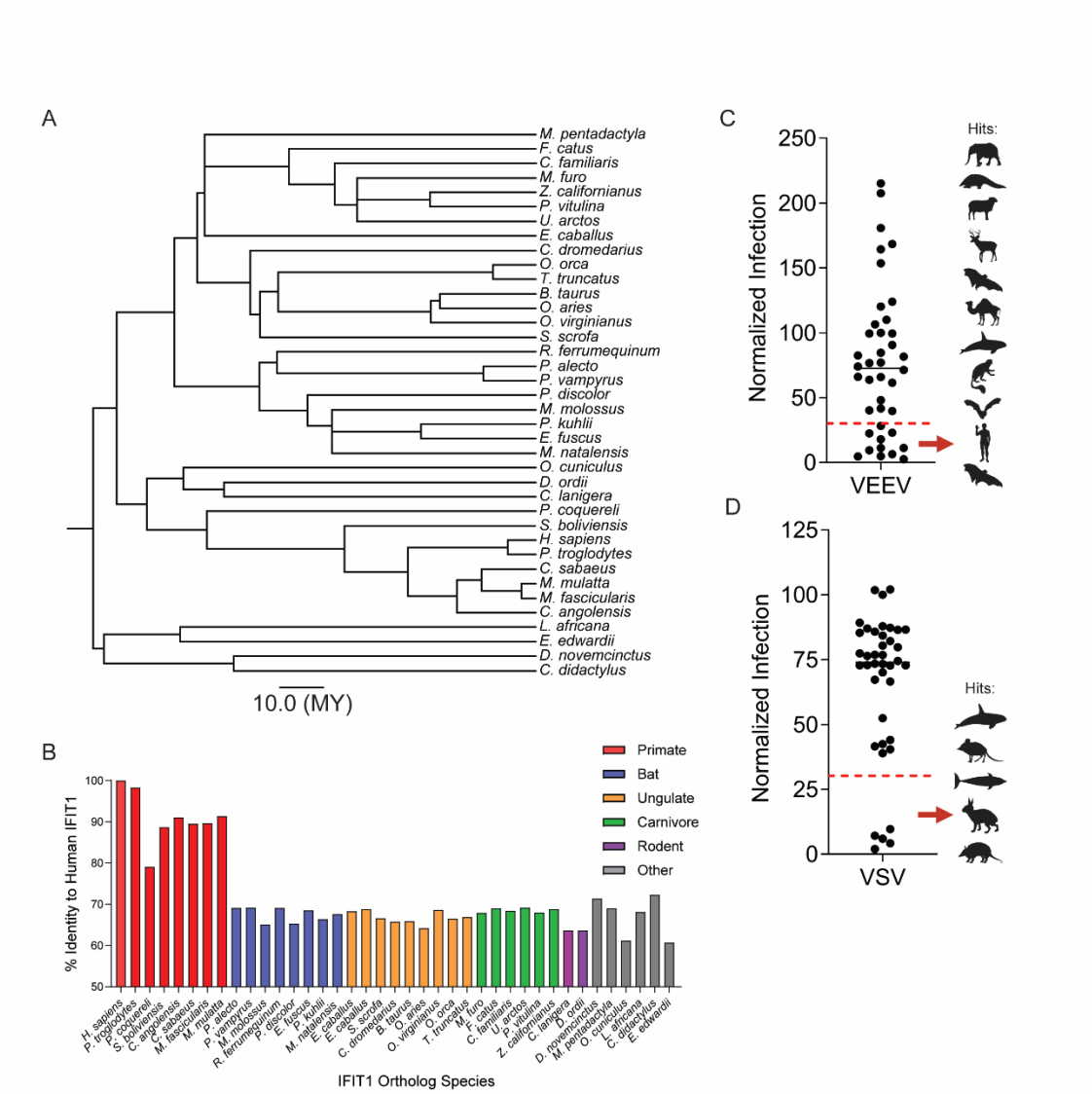

Figure 3. IFIT1 ortholog screens reveal extensive heterogeneity in mammalian IFIT1 antiviral function. A. TimeTree illustrating the evolutionary relationship of IFIT1 orthologs selected for ortholog screen. Scale bar represents divergence time of 10 million years. B. Graph of protein sequence identity of IFIT1 orthologs used in screen relative to human IFIT1. C. Dot plot representing the relative infection (compared to control cells) from an ectopic overexpression screen in which Huh7.5 cells expressing 39 different IFIT1 mammalian orthologs were challenged with 1.0 MOI VEEV-GFP for 4 h. Infectivity was quantified by flow cytometry. Red line denotes 30% relative infection. n=2 biological replicates. D. Same as C, for VSV-GFP (1 MOI, 4 h infection). n=3 biological replicates.

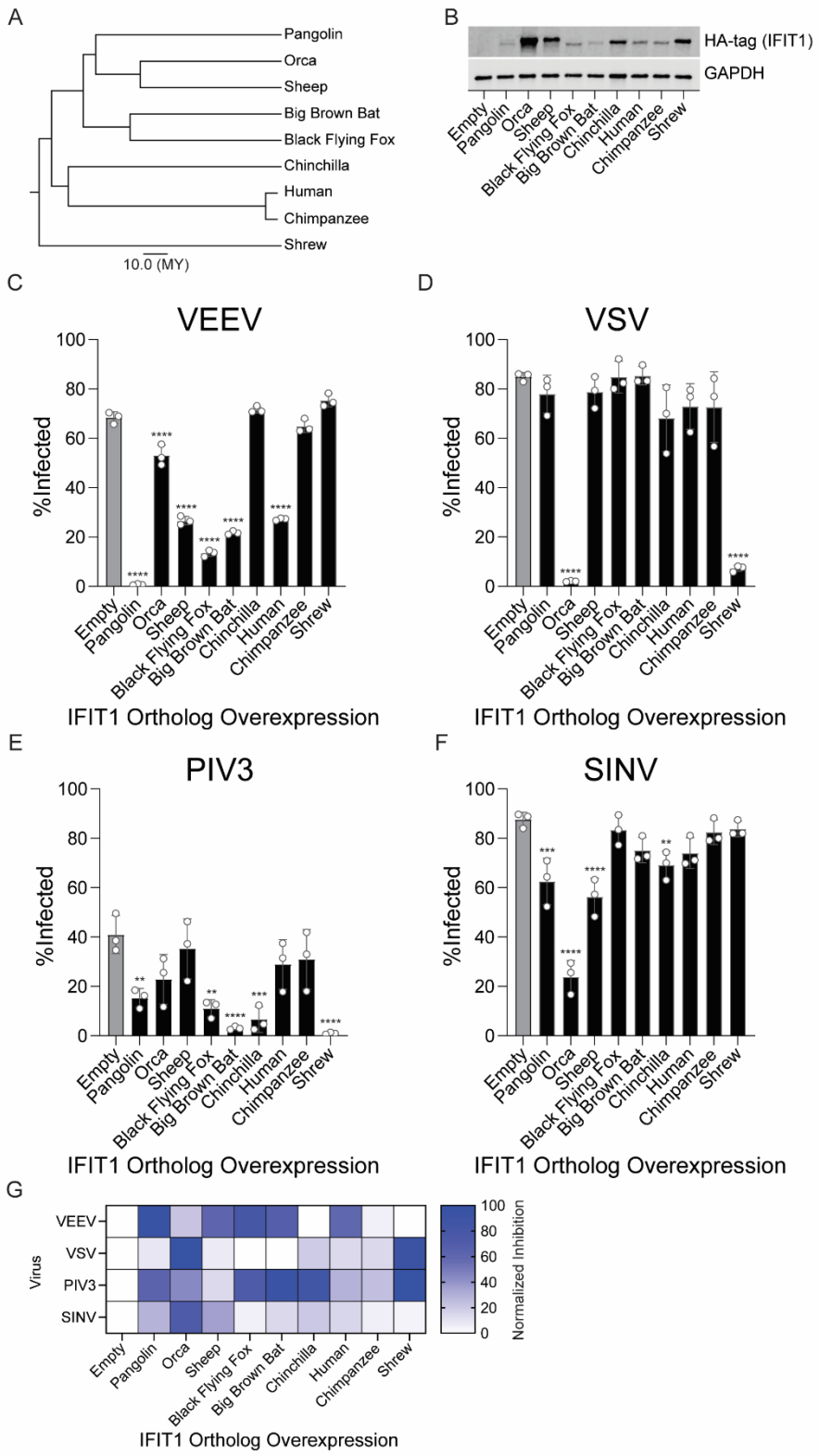
A
Pangolin
Orca
Sheep
Big Brown Bat
Black Flying Fox
Chinchilla
Human
Chimpanzee
Shrew
10.0 (MY)
B
HA-tag (IFIT1)
GAPDH
Empty
Pangolin
Orca
Sheep
Black Flying Fox
Big Brown Bat
Chinchilla
Human
Chimpanzee
Shrew
C
VEEV
%Infected
IFIT1 Ortholog Overexpression
D
VSV
%Infected
IFIT1 Ortholog Overexpression
E
PIV3
%Infected
IFIT1 Ortholog Overexpression
F
SINV
%Infected
IFIT1 Ortholog Overexpression
G
Virus
VEEV
VSV
PIV3
SINV
Normalized Inhibition
IFIT1 Ortholog Overexpression

646

Figure 4. Validation of selected IFIT1s from ortholog screen. A. TimeTree illustrating the evolutionary relationship of IFIT1 orthologs selected for screen validation and follow-up. Scale bar represents divergence time of 10 million years. B. Western blot from cells expressing HA-tagged IFIT1 orthologs used in C-F. Image is representative of three independent replicates. C. Infection of IFIT1 ortholog-expressing Huh7.5 cells with VEEV-GFP (MOI 2, 4h) D. Infection of IFIT1 ortholog-expressing Huh7.5 cells with VSV-GFP (MOI 2, 4h) E. Infection of IFIT1 ortholog-expressing Huh7.5 cells with PIV3-GFP (MOI 2, 10h) F. Infection of IFIT1 ortholog-expressing Huh7.5 cells with SINV-GFP (MOI 2, 10h). In C-F, data represent mean ± SD, n=3 biological replicates. Statistical significance was determined by one-way ANOVA with Dunnett's test. ns $p > 0.05$, **$p < 0.01$, ***$p < 0.001$, and ****$p < 0.0001$.

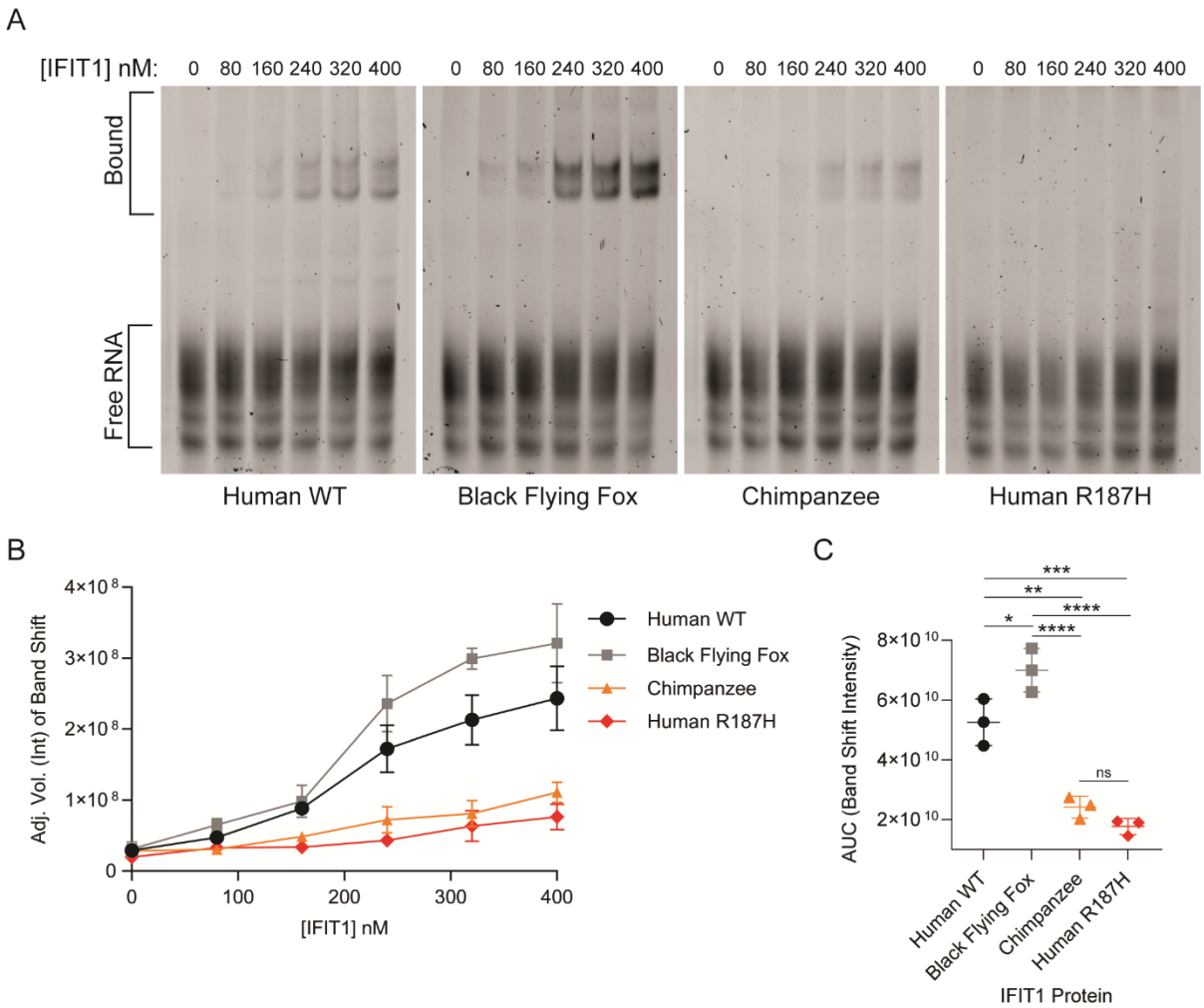

Figure 5. IFIT1 proteins exhibit species-specific Cap0 RNA binding. A. RNA EMSA with Cap0 VEEV RNA probes (41nt of VEEV TC-83 strain 5' UTR) at 50nM incubated with increasing concentrations of the indicated purified IFIT1 proteins. Images are one representative image from three independent replicates. B. Plot of the band shift intensity from EMSAs in A. Data represent mean ± SD, n=3. Band intensity was quantified by ImageLab software (BioRad). C. Area Under the Curve (AUC) analysis calculated from raw data in B. Statistical significance was tested by one-way ANOVA with correction for multiple comparisons. Data represent mean ± SD, n=3 replicates. ns, $p > 0.05$, *, $p < 0.05$, **, $p < 0.01$, ***, $p < 0.001$, and **** $p < 0.0001$.

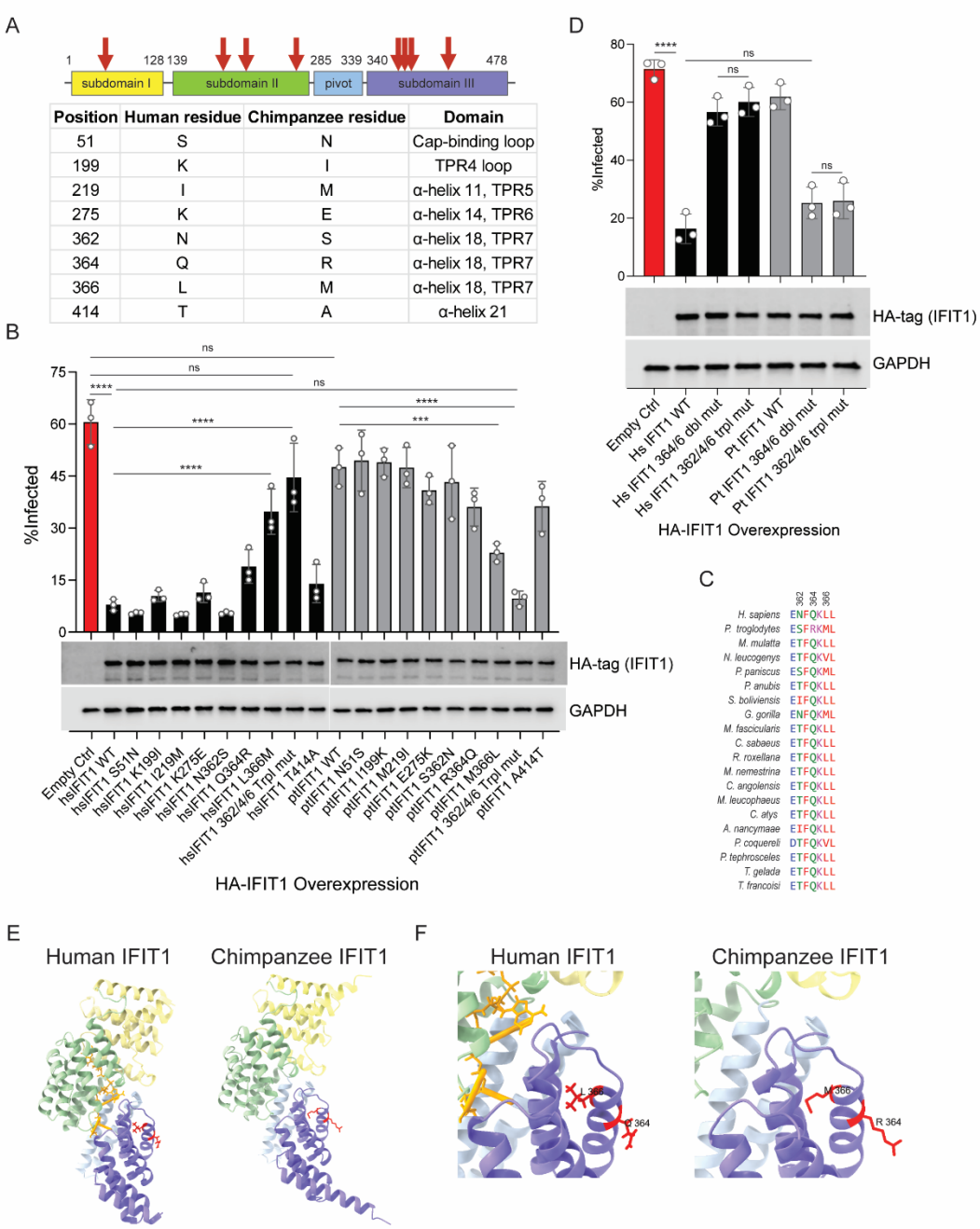

Figure 6. Mutagenesis uncovers genetic determinants of primate IFIT1 antiviral function. A. Diagram and chart describing amino acids that differ between human and chimpanzee IFIT1 as well as their domain location. B. Effects of primate IFIT1 mutant expression on VEEV-GFP infection. Huh7.5 cells were infected with an MOI of 2 for 4 h and infectivity was quantified by flow cytometry. Data represent mean ± SD, n=3 biological replicates. Statistical significance was determined by one-way ANOVA with Dunnett's test. ns, $p > 0.05$; ***, $p < 0.001$; and **** $p < 0.0001$. Western blotting for HA-tag (IFIT1) and GAPDH (Loading control) was also performed to determine expression levels of IFIT1 mutants. C. ClustalOmega protein sequence alignment of residues 361-367 of IFIT1 from 20 primate species. D. Effects of primate IFIT1 double or

683 triple mutants on VEEV-GFP infection. Huh7.5 cells were infected with an MOI of 2 for 4 h and
684 infectivity was quantified by flow cytometry. Data represent mean ± SD, n=3 biological
685 replicates. Statistical significance was determined by one-way ANOVA with Dunnett's test. ns, p
686 > 0.05; and **** $p < 0.0001$. Western blotting for HA-tag (IFIT1) and GAPDH (Loading control)
687 was also performed to determine relative IFIT1 mutant protein abundance. E. Structure of
688 human IFIT1 bound to RNA (left) or AlphaFold predicted structure of chimpanzee IFIT1 (right)
689 visualizing location of residues 364 and 366 (red) that confer antiviral activity. Graphics were
690 generated using ChimeraX. F. Zoom in of (E).

A

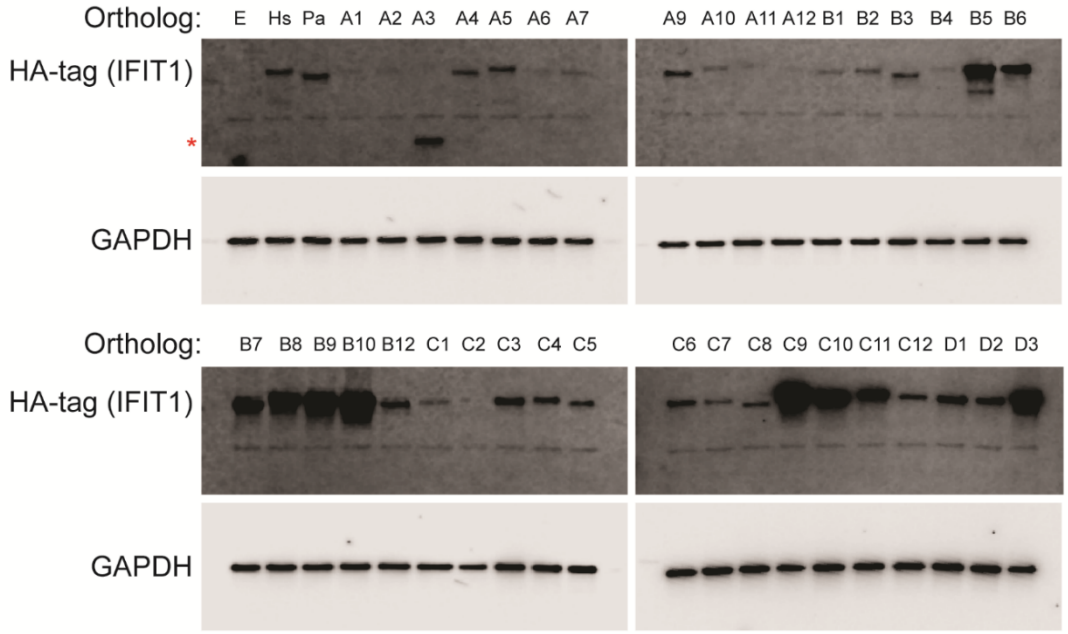

B

Common Name	Scientific Name	Key	Common Name	Scientific Name	Key
Empty Control	N/A	E	Cow	*Bos taurus*	B7
Human	*Homo sapiens*	Hs	Sheep	*Ovis aries*	B8
Black flying fox	*Pteropus alecto*	Pa	White-tailed deer	*Odocoileus virginianus texanus*	B9
African green monkey	*Chlorocebus sabaeus*	A1	Killer whale	*Orcinus orca*	B10
Coquerel's sifaka	*Propithecus coquereli*	A2	Common bottlenose dolphin	*Tursiops truncatus*	B12
Black-capped squirrel monkey	*Saimiri boliviensis*	A3	Ferret	*Mustela putorius furo*	C1
Angola colobus	*Colobus angolensis*	A4	Cat	*Felis catus*	C2
Chimpanzee	*Pan troglodytes*	A5	Dog	*Canis lupus familiaris*	C3
Crab-eating macaque	*Macaca fascicularis*	A6	Grizzly bear	*Ursus arctos horribilis*	C4
Rhesus macaque	*Macaca mulatta*	A7	Harbor (common) seal	*Phoca vitulina*	C5
Large flying fox	*Pteropus vampyrus*	A9	California sea lion	*Zalophus californianus*	C6
Velvety free tailed bat	*Molossus molossus*	A10	Nine-banded armadillo	*Dasypus novemcinctus*	C7
Greater horseshoe bat	*Rhinolophus ferrumequinum*	A11	Chinese pangolin	*Manis pentadactyla*	C8
Pale spear-nosed bat	*Phyllostomus discolor*	A12	European rabbit	*Oryctolagus cuniculus*	C9
Big brown bat	*Eptesicus fuscus*	B1	African savannah elephant	*Loxodonta africana*	C10
Kuhl's pipistrelle	*Pipistrellus kuhlii*	B2	Cape elephant shrew	*Elephantulus edwardii*	C11
Natal long-fingered bat	*Miniopterus natalensis*	B3	Linnaeus's two-toed sloth	*Choloepus didactylus*	C12
Horse 1	*Equus caballus*	B4	Ord's kangaroo rat	*Dipodomys ordii*	D1
Pig	*Sus scrofa*	B5	Chinchilla	*Chinchilla lanigera*	D2
Dromedary camel	*Camelus dromedarius*	B6	Horse 2	*Equus caballus*	D3

Supplementary Figure 1. IFIT1 ortholog expression varied during the ortholog screen. A. Western blot from lysates of cells expressing HA-tagged IFIT1 orthologs for screen in Fig 1A demonstrating unequal IFIT1 expression patterns. Images are representative of three independent replicates. B. Key denoting which symbols correspond to HA-tagged IFIT1 ortholog. Red asterisk marks the size of the truncated or cleaved protein product in lane A3.

697

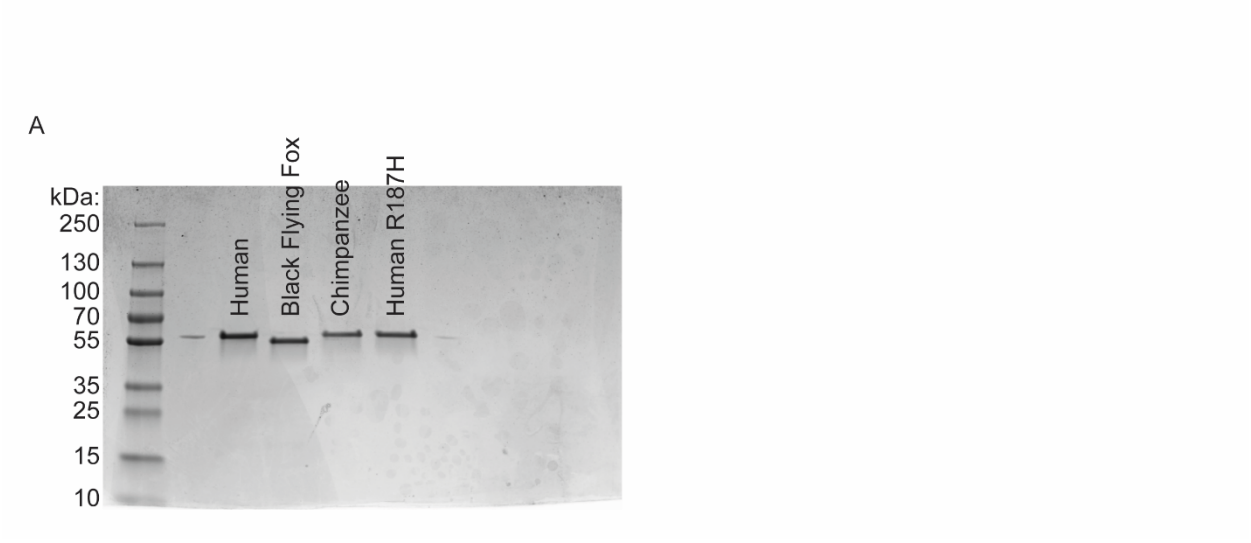

698

699

700 **Supplementary Figure 2. Gel image of recombinant IFIT1 protein.** A. Coomassie stained
701 SDS-PAGE gel of purified IFIT1 protein used for RNA EMSA.

References

1. Hyde JL, Gardner CL, Kimura T, White JP, Liu G, Trobaugh DW, et al. A viral RNA structural element alters host recognition of nonself RNA. Science. 2014;343(6172):783-7.
2. Pichlmair A, Lassnig C, Eberle CA, Gorna MW, Baumann CL, Burkard TR, et al. IFIT1 is an antiviral protein that recognizes 5'-triphosphate RNA. Nat Immunol. 2011;12(7):624-30.
3. Abbas YM, Laudenbach BT, Martinez-Montero S, Cencic R, Habjan M, Pichlmair A, et al. Structure of human IFIT1 with capped RNA reveals adaptable mRNA binding and mechanisms for sensing N1 and N2 ribose 2'-O methylations. Proc Natl Acad Sci U S A. 2017;114(11):E2106-E15.
4. Diamond MS, Farzan M. The broad-spectrum antiviral functions of IFIT and IFITM proteins. Nat Rev Immunol. 2013;13(1):46-57.
5. Hyde JL, Diamond MS. Innate immune restriction and antagonism of viral RNA lacking 2-O methylation. Virology. 2015;479-480:66-74.
6. Daugherty MD, Malik HS. Rules of engagement: molecular insights from host-virus arms races. Annu Rev Genet. 2012;46:677-700.
7. Duggal NK, Emerman M. Evolutionary conflicts between viruses and restriction factors shape immunity. Nat Rev Immunol. 2012;12(10):687-95.
8. Sironi M, Cagliani R, Forni D, Clerici M. Evolutionary insights into host-pathogen interactions from mammalian sequence data. Nat Rev Genet. 2015;16(4):224-36.
9. Mitchell PS, Patzina C, Emerman M, Haller O, Malik HS, Kochs G. Evolution-guided identification of antiviral specificity determinants in the broadly acting interferon-induced innate immunity factor MxA. Cell Host Microbe. 2012;12(4):598-604.
10. Sawyer SL, Wu LI, Emerman M, Malik HS. Positive selection of primate TRIM5alpha identifies a critical species-specific retroviral restriction domain. Proc Natl Acad Sci U S A. 2005;102(8):2832-7.
11. Daugherty MD, Schaller AM, Geballe AP, Malik HS. Evolution-guided functional analyses reveal diverse antiviral specificities encoded by IFIT1 genes in mammals. Elife. 2016;5.
12. Cruz-Rivera PCDL, Eitson JL, Schoggins JW. IRF7 from the black flying fox induces a STAT1-independent ISG response in unstimulated cell lines that protects against diverse RNA viruses. bioRxiv. 2024:2024.05.02.592239.
13. Yang Z. PAML 4: phylogenetic analysis by maximum likelihood. Mol Biol Evol. 2007;24(8):1586-91.
14. Murrell B, Moola S, Mabona A, Weighill T, Sheward D, Kosakovsky Pond SL, et al. FUBAR: a fast, unconstrained bayesian approximation for inferring selection. Mol Biol Evol. 2013;30(5):1196-205.
15. Murrell B, Wertheim JO, Moola S, Weighill T, Scheffler K, Kosakovsky Pond SL. Detecting individual sites subject to episodic diversifying selection. PLoS Genet. 2012;8(7):e1002764.
16. Reynaud JM, Kim DY, Atasheva S, Rasalouskaya A, White JP, Diamond MS, et al. IFIT1 Differentially Interferes with Translation and Replication of Alphavirus Genomes and Promotes Induction of Type I Interferon. PLoS Pathog. 2015;11(4):e1004863.
17. Andrejeva J, Norsted H, Habjan M, Thiel V, Goodbourn S, Randall RE. ISG56/IFIT1 is primarily responsible for interferon-induced changes to patterns of parainfluenza virus type 5 transcription and protein synthesis. J Gen Virol. 2013;94(Pt 1):59-68.
18. Halpin K, Young PL, Field HE, Mackenzie JS. Isolation of Hendra virus from pteropid bats: a natural reservoir of Hendra virus. J Gen Virol. 2000;81(Pt 8):1927-32.
19. Marsh GA, de Jong C, Barr JA, Tachedjian M, Smith C, Middleton D, et al. Cedar virus: a novel Henipavirus isolated from Australian bats. PLoS Pathog. 2012;8(8):e1002836.
20. Barr JA, Smith C, Marsh GA, Field H, Wang LF. Evidence of bat origin for Menangle virus, a zoonotic paramyxovirus first isolated from diseased pigs. J Gen Virol. 2012;93(Pt 12):2590-4.

21. Boys IN, Xu E, Mar KB, De La Cruz-Rivera PC, Eitson JL, Moon B, et al. RTP4 Is a Potent IFN-Inducible Anti-flavivirus Effector Engaged in a Host-Virus Arms Race in Bats and Other Mammals. Cell Host Microbe. 2020;28(5):712-23 e9.
22. Chan SH, Mole CN, Nye D, Mitchell L, Dai N, Buss J, et al. Biochemical characterization of mRNA capping enzyme from Faustovirus. RNA. 2023;29(11):1803-17.
23. Fensterl V, Sen GC. Interferon-induced Ifit proteins: their role in viral pathogenesis. J Virol. 2015;89(5):2462-8.
24. Tenthorey JL, Young C, Sodeinde A, Emerman M, Malik HS. Mutational resilience of antiviral restriction favors primate TRIM5alpha in host-virus evolutionary arms races. Elife. 2020;9.
25. Atasheva S, Krendelchtchikova V, Liopo A, Frolova E, Frolov I. Interplay of acute and persistent infections caused by Venezuelan equine encephalitis virus encoding mutated capsid protein. J Virol. 2010;84(19):10004-15.
26. Simmons JD, Wollish AC, Heise MT. A determinant of Sindbis virus neurovirulence enables efficient disruption of Jak/STAT signaling. J Virol. 2010;84(21):11429-39.
27. Kane M, Zang TM, Rihn SJ, Zhang F, Kueck T, Alim M, et al. Identification of Interferon-Stimulated Genes with Antiretroviral Activity. Cell Host Microbe. 2016;20(3):392-405.
28. Kumar S, Stecher G, Li M, Knyaz C, Tamura K. MEGA X: Molecular Evolutionary Genetics Analysis across Computing Platforms. Mol Biol Evol. 2018;35(6):1547-9.
29. Castresana J. Selection of conserved blocks from multiple alignments for their use in phylogenetic analysis. Mol Biol Evol. 2000;17(4):540-52.
30. Glez-Pena D, Gomez-Blanco D, Reboiro-Jato M, Fdez-Riverola F, Posada D. ALTER: program-oriented conversion of DNA and protein alignments. Nucleic Acids Res. 2010;38(Web Server issue):W14-8.
31. Murrell B, Weaver S, Smith MD, Wertheim JO, Murrell S, Aylward A, et al. Gene-wide identification of episodic selection. Mol Biol Evol. 2015;32(5):1365-71.
32. Kosakovsky Pond SL, Poon AFY, Velazquez R, Weaver S, Hepler NL, Murrell B, et al. HyPhy 2.5-A Customizable Platform for Evolutionary Hypothesis Testing Using Phylogenies. Mol Biol Evol. 2020;37(1):295-9.
33. Weaver S, Shank SD, Spielman SJ, Li M, Muse SV, Kosakovsky Pond SL. Datamonkey 2.0: A Modern Web Application for Characterizing Selective and Other Evolutionary Processes. Mol Biol Evol. 2018;35(3):773-7.
34. Kumar S, Stecher G, Suleski M, Hedges SB. TimeTree: A Resource for Timelines, Timetrees, and Divergence Times. Mol Biol Evol. 2017;34(7):1812-9.
35. Sievers F, Wilm A, Dineen D, Gibson TJ, Karplus K, Li W, et al. Fast, scalable generation of high-quality protein multiple sequence alignments using Clustal Omega. Mol Syst Biol. 2011;7:539.
36. Meng EC, Goddard TD, Pettersen EF, Couch GS, Pearson ZJ, Morris JH, et al. UCSF ChimeraX: Tools for structure building and analysis. Protein Sci. 2023;32(11):e4792.